Stiff response of Aluminum under ultra-fast shockless compression to 110 GPa

Raymond F. Smith[1], Jon H. Eggert[1], Alan Jankowski[1], Peter M. Celliers[1], M. John Edwards[1], Yogendra M. Gupta[2], James R. Asay[2], Gilbert W. Collins[1]

[1]*Lawrence Livermore National Laboratory, P.O. Box 808, CA 94550*
[2]*Washington State University, Pullman, Wa 99164*

A laser produced x-ray drive was used to shocklessly compress solid aluminum to a peak longitudinal stress of 110 GPa within 10 ns. Interface velocities versus time for multiple sample thicknesses were measured and converted to stress-density (P_x–ρ) using an iterative Lagrangian analysis. These are the fastest shockless compression $P_x(\rho)$ results reported to date, and are stiffer than models that have been benchmarked against both static and shock wave experiments. The present results suggest that at these short time scales, there is a higher stress-dependent strength, and a stiffer time-dependent inelastic response than had been expected.

Understanding condensed matter response at extreme compressions is an important element of contemporary research in physics and materials science. Two common approaches to achieving large compressions in laboratory experiments involve static compression using diamond-anvil-cells (DAC) and dynamic compression using shock-wave-compression methods. Both approaches provide information along limited regions of the complete equation-of-state (EOS) surface of a material and monitor material response over very different timescales. DAC experiments typically provide isothermal data up to a pressure range of 200-300 GPa [1] with experimental timescales of seconds to days. Shock wave experiments, depending upon the method, can provide data up to several TPa [2] with timescales ranging from subnanosecond to microsecond. Shock compression produces a significant temperature increase so that at high pressures ($\geq$100 GPa) they sample very different regions of thermodynamic space than DAC experiments. The development of a complete EOS and understanding of high-pressure material response by comparing DAC and shock wave results has long been an active area of experimental and theoretical research.

Recent experiments have demonstrated the production and propagation of high-stress ramp waves that result in quasi-isentropic compression of condensed materials [3-6]. This permits the sampling of thermodynamic space not accessible by shock wave or static pressure methods, ensures a solid state even at very high pressures, and provides and intermediate link between shock wave and static pressure results. Depending on the ramp-wave-loading method, rise times can be varied between tens of nanoseconds to several microseconds. This capability enables the study of time-dependent material behavior associated with structural changes and deformation in solids subjected to

extreme compressions. Studies of time-dependent material response typically have used shock wave experiments, in which the material is subjected to step loading. Under such loading, compression consists of elastic and inelastic deformation and stress relaxation occurs on a timescale associated with lattice-dislocation mobility. At low stresses, an elastic wave, with a thickness-dependent amplitude, runs ahead of the plastic wave. At high stresses, a steady plastic wave emerges with a rise time determined by a competition between the non-linear stress-strain response and dissipative behavior [7].

What is the stress-strain response of a material dynamically compressed on a timescale comparable to the steady-shock rise time? The laser-driven ramp-compression experiments (commonly referred to as quasi-isentropic compression experiments, or ICE) described here uniaxially compress a material by applying a monotonically increasing stress over ~10 nanoseconds, which is comparable to the low-stress steady-shock rise time for aluminum as reported by Swegle and Grady [7]. The ability to shocklessly compress materials to very high stresses on timescales comparable to dissipative relaxation times permits a new approach to explore the time-dependent deformation of materials at extreme conditions.

Shockless pressure loading techniques have been demonstrated using several drivers such as magnetic-pulse loading [3, 8, 11], graded-density impactors on gas guns facilities [4], chemical energy of high explosives [5], and lasers [6, 9]. The characteristic loading time for magnetic ramp loading is ~100 ns, for graded-density-impactor loading is ~μs, and for laser ramp loading is ~10 ns. Here we present the most rapidly compressed, shockless P_x–ρ results obtained to date. These new quasi-isentropic data reveal a stiffer response than expected from current EOS models and strength data.

Shockless compressions at these short time-scales also produce precursor waves with amplitudes significantly higher than previously reported in shock and slower ramp compression experiments. By comparing in-situ and free-surface measurements, the results presented here provide a good test of the release correction using the iterative Lagrangian wave profile analysis and the reproducibility of ramp-loading experiments.

In previous laser-driven shockless compression experiments [6, 9], the planarity of the pressure loading was limited by laser focal-spot smoothing techniques, which precluded their use for EOS measurements. Here, we have developed a laser-produced x-ray drive technique to generate ramp-wave loading that was spatially uniform to < 1% over 500 μm. This uniform loading ensured that different thicknesses of multi-step targets had the same loading history. A target layout is shown in Fig. 1(a). Fifteen beams from the Omega laser, with a combined energy of up to 5.9 kJ in a 2ns temporally-flat pulse, were focused onto the inner walls of an Au hohlraum. This generated a uniform distribution of thermal x-rays with a peak radiation temperature, $T_r = 135$ eV as measured with a calibrated array of filtered diodes. An ablatively-driven shock runs through a 180μm-thick, 12% Br-doped polystyrene foil [$C_8H_6Br_2$]. After shock breakout from the rear surface, the CH-Br unloading plasma crosses a ~ 400 μm vacuum gap and piles up against the multi-step Al sample launching a ramped stress wave. The vacuum gap, T_r, and Al thicknesses were tuned to optimize the pressure and accuracy. The Bromine dopant absorbs high energy Au M-band x-rays generated within the hohlraum which otherwise could pre-heat the Al step sample. The level of x-ray preheat was determined to be negligible by measuring the thermal expansion velocity of a thin Al foil under the target and irradiation conditions described here.

Al samples were either a 10, 20, and 30 μm thick stepped foil attached to a LiF window or a 40, 60, and 80 μm free-standing stepped foil. For Al/LiF samples, Al was coated directly onto stepped LiF windows with electron-beam deposition at a growth temperature of 425 K. For free-standing samples, Al was deposited onto a salt mandrel in a similar way and then the mandrel was removed. Optical imaging of the samples showed a tightly packed ~5 μm long tapered crystallite structure in the stress-loading direction with an average in-plane grain size of ~1.5 ± 0.3 μm. Bragg diffraction showed a preferential [111] FCC structure in the growth direction. Samples were measured to be fully dense (2.7 g/cc) to within an accuracy of -0.6%. After deposition, the Al surface away from the mandrel was diamond turned to achieve planarity. Through each stage of the process, white-light interferometry was used to ensure a surface roughness < 0.1μm, overall thickness gradients < 1%, and step heights < 1%. The high purity LiF was oriented with the [100] axis along the pressure loading direction [12].

As the particle-velocity wave reaches the back surface of the Al, it begins to accelerate into the LiF window or into free space. The interface-velocity history $u_{Al/LiF}$ or u_{fs}, is recorded with a line-imaging velocity interferometer (VISAR) with two channels set at different sensitivities [13]. Figure 1(b) insert shows a typical streak camera output of the VISAR for an Al/LiF target. The spatial resolution is ~5μm over ~500μm at the target plane. The temporal resolution is 50 ps over a 30ns time window. The minimum velocity per fringe was 0.645 km s^{-1} and we detect fringe position to 5% of a fringe. Figure 1(b) shows representative interface-velocity histories for each of the 10, 20 and 30 μm thick steps. For all Al/LiF samples, we observed a low amplitude precursor similar to the elastic precursor in shock experiments [14]. This velocity plateau corresponds to

$P_x \sim 2.7$ GPa, which is significantly higher than the reported Hugoniot Elastic Limit (HEL) for pure Al (~ 0.4 GPa) on millimeter-scale thick targets [14] and seventeen times higher than quasi-static tensile measurements on the same material used here.

An iterative characteristic method outlined by Maw and Rothman [15] is used to convert interface-velocity histories to particle velocity, u. One central assumption for all current ramp-wave-analysis techniques is that the ramp wave is a simple wave. This implies [16] that the stress and particle-velocity propagation speeds are identical and equal to $C_L(u)$. For Al/LiF targets, the measured interface velocity is very close to the in-situ particle velocity due to the comparable mechanical impedance of LiF and Al. Furthermore, the refractive index of LiF depends linearly on density in this regime, so the index correction for the velocity calibration is trivial [17]. However, late in time a shock forms in the LiF producing a release fan, which propagates back to, and accelerates the Al/LiF interface. At this point the analysis becomes more difficult and so was terminated for these experiments. The open circles Fig. 1(b) show where the release from shock formation in the LiF reaches the Al/LiF interface, as determined from the characteristic analysis. For Al/vacuum targets, release waves from the Al/vacuum interface significantly perturb the incoming ramp wave. Extensive tests using simulated data confirm that the iterative Lagrangian analysis accurately corrects for these wave interactions. When the release wave reflects from the drive surface and reaches the Al/vacuum interface again, the analysis is stopped due to an increase in velocity that is not accounted for with present analysis techniques.

The iterative Lagrangian analysis gives a time for a given particle velocity, u, to reach each step. The Lagrangian sound speed, $C_L(u)$, and its uncertainty, $\sigma_{CL}(u)$, are

obtained from this position-time data by linear regression using errors determined by measurements accuracies: Up (~0.1 km/s), time (~50ps), step height (~1%). $C_L(u)$ for each of the 7 independent experiments (5 with LiF windows and 2 free surfaces) taken over three different shot days are shown as insert in Fig. 2. To our knowledge, the present work represents the first comparison of different ramp-loading experiments to evaluate systematics. That the Al/vacuum and Al/LiF targets yield the same value for $C_L(u)$, demonstrates that the methodology for correcting for the strong release effects is indeed consistent.

Also shown in the fig. 2 insert is the weighted mean,

$$\overline{C_L(u)} = \sum_j \frac{C_{L,j}}{\sigma_{CL,j}^2} \bigg/ \sum_i \frac{1}{\sigma_{CL,j}^2} \text{, and uncertainty in the mean, } \sigma_{\overline{CL(u)}} = \left(1 \bigg/ \sum_j \frac{1}{\sigma_{CL,j}^2} \right)^{\frac{1}{2}}. \text{ For}$$

$u > 0.5$ km/s the weighted mean can be linearly extrapolated to a value close to the bulk sound speed (open circle) [1]. For values of $u < 0.5$ the weighted mean extrapolates closer to the longitudinal sound speed (green circle) [18]. For particle speeds < 0.2 km/s, C_L is dominated by elastic deformation.

$\overline{C_L(u)}$ and $\sigma_{\overline{CL(u)}}$ are integrated [15, 16] to obtain, $P_x = \rho_0 \int_0^u \overline{C_L(u)} du$,

$$\rho = \left(\frac{1}{\rho_0} - \int_0^u \frac{du}{\rho_0 \overline{C_L(u)}} \right)^{-1}, \quad \text{and} \quad \text{their} \quad \text{uncertainties,} \quad \sigma_{P_x} = \rho_0 \int_0^u \sigma_{\overline{CL(u)}} du,$$

$\sigma_\rho = \rho^2 \int_0^u \frac{\sigma_{\overline{CL(u)}} du}{\rho_0 \overline{C_L(u)}^2}$. Uncertainties are propagated through the integrals linearly, rather than in quadrature, because $\sigma_{\overline{CL(u)}}$ appears to be correlated rather than random over the

ramp wave. This method of uncertainty propagation allows the direct propagation of experimental uncertainties to the P_x-ρ density relation.

The resultant P_x versus ρ are shown in Fig. 2. Stress-density results reported here are stiffer than results recently published from pulsed power experiments by Hayes [8] and Davis [11]. One possible reason for this difference is that our ramp times (~10 ns) and thicknesses (~10's of microns) are 10 to 100 times less than previous ramp-wave compression experiments and our compression times are similar to the steady wave rise times under shock loading. Also shown for comparison are Hugoniot results from several authors [2], the cold curve from Dewale *et al.* [19], and the isentrope calculated from the EOS model 3700 and 3719 both from the Sesame database [20]. Sesame 3700 has previously been shown to give good agreement with Hugoniot data up to several hundred GPa [21].

Figure 3 accentuates the differences shown in Fig. 2, by plotting the difference between the P_x values and the isentrope calculated from the Sesame 3700 EOS table. For an elastic-plastic solid, the longitudinal stress differs from the corresponding mean stress (here, the calculated isentrope) by 2/3 times the equilibrium flow strength [14]. Thus, assuming that the isentrope calculated using Sesame 3700 is correct, and the additional longitudinal stress is dominated by strength effects, the maximum value for the flow strength can be obtained in Figure 3 by reading off the right hand axis. Also plotted in Fig. 3 are flow-strength data from several authors. The stress difference observed in the present experiments is higher than expected from shock-wave strength determinations by Huang and Asay [22], Altshuler [23], and ramp-load results of Lorenz *et al.* [10] but lower than expected from results of Batkov [24]. While the Batkov results are

systematically high compared to other results, the difference between their ramp and shock results are comparable to the difference between our ramp-load results and the shock results in refs. [22] and [23].

In summary, results presented here represent a systematic study of the quasi-isentropic behavior of Al at strain rates approaching 10^8/s [25], and provide P_x–ρ results to 100 GPa. In the predominately plastic regime, P_x is larger than expected by ~6-8 GPa at ~100 GPa, suggesting a higher stress-dependent strength and a larger than expected time-dependent deformation response at these short time scales. In addition, the elastic precursor stress for Al/LiF samples is nearly seven times higher than previously reported in ramp- and shock-wave experiments [26]. Further experimental, analytical, and theoretical work is needed to understand the results presented here. However, it is clear that ramp-wave experiments, with rise times comparable to material dissipation times have the potential to provide new insights into the dynamic response of materials at extreme conditions.

References

[1]   A.D. Chijioke *et al.*, J. Appl. Phys. **98**, 073526 (2005).

[2]   See P.M. Celliers *et al.*, J. Appl. Phys. **98,** 113529 (2005) and references within.

[3]   R.S. Hawke *et al.*, J. Appl. Phys. **43**, 2734 (1972); J.R. Asay, AIP Conf. Proc. **505**, 261 (2000).

[4]   L.C. Chhabildas and L.M. Barker, Sandia Report SAND86-1888 (1986); J.R. Asay, Int. J. Impact Engng. **20**, 27 (1997).

[5]   J.F. Barnes *et al.*, J. Appl. Phys. **45**, 727 (1974).

[6]   M.J. Edwards *et al.*, Phys. Rev. Lett. **92**, 075002/1 (2004).

[7]   J.W. Swegle and D.E. Grady, J. Appl. Phys. **58**, 692 (1985).

[8]   D.B. Hayes *et al.*, J. App. Phys. **96**, 5520 (2004).

[9]   D.C. Swift and R.P. Johnson, Phys. Rev. E **71**, 066401 (2005).

[10] K.T. Lorenz *et al.*, Phys. Plas. **12**, 056309 (2005).

[11] J-P Davis, J. App. Phys. **99**, 103512 (2006).

[12] J.L. Wise and L.C. Chhabildas, Shock waves in condensed matter – 1985, Y.M. Gupta, ed., p. 441, Plenum, New York, (1986).

[13] P.M. Celliers *et al.*, Rev. Sci. Instrum. **75**, 4916 (2004).

[14] J.N. Johnson and L.M. Barker, J. Appl. Phys. **40**, 4321 (1969).

[15] J.R. Maw, AIP Conf. Proc. **706**, 1217 (2004); S.D. Rothman *et al.*, J. Phys. D: Appl. Phys. **38**, 733 (2005).

[16] J.B. Aidun and Y.M. Gupta, J. Appl. Phys. **69**, 6998 (1991); R. Fowles and R.F. Williams, J. Appl. Phys. **41**, 360 (1970); M. Cowperthwait and R.F. Williams, J. Appl. Phys. **42**, 456 (1971).

[17] D.B. Hayes, J. App. Phys. **89**, 6484 (2001).

[18] S. Marsh, *LASL Shock Hugoniot Data*, University of California Press, (1980).

[19] A. Dewaele *et al.*, Phys. Rev. B **70**, 094112 (2004).

[20] G.I. Kerley, Int. J. Impact Eng. **5**, 441 (1987); S. P. Lyon and J. D. Johnson, *T-1 Handbook of the* SESAME *Equation of State Library*, Vols. 1 and 2, Los Alamos Report LA-CP-98-100, 1998. The Al EOS developed by G. Kerley is used at the Sandia National Laboratories and commonly referred to as the 3700 table.

[21] M.D. Knudson *et al.*, J. Appl. Phys. **97**, 073514 (2005).

[22] H. Huang and J.R. Asay, J. Appl. Phys. **98**, 33524 (2005).

[23] L.V. Al'tshuler, Comb. Expl. and Shock waves, **35**, 92 (1999).

[24] Y.V. Bat'kov *et al*., AIP Conference Proceedings **505**, 501 (2000).

[25] The strain rate, $d(\eta)/d(t) \equiv [d(u)/d(t)]/[C_L(u)]$, where the strain ($\eta$) is positive under compression and u is the particle velocity, we find $d(\eta)/d(t)$ increases from 10^6/sec at a few GPa to 10^8/sec at ~5 GPa then drops slowly above 5 GPa.

[26] The previous experiments used Al 6061 with a grain size of a few hundred μm in contrast to the pure Al with ~ 5 μm columnar crystals used in this study.
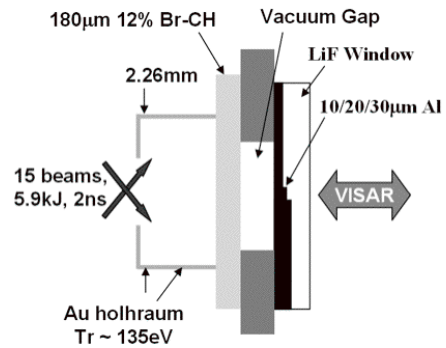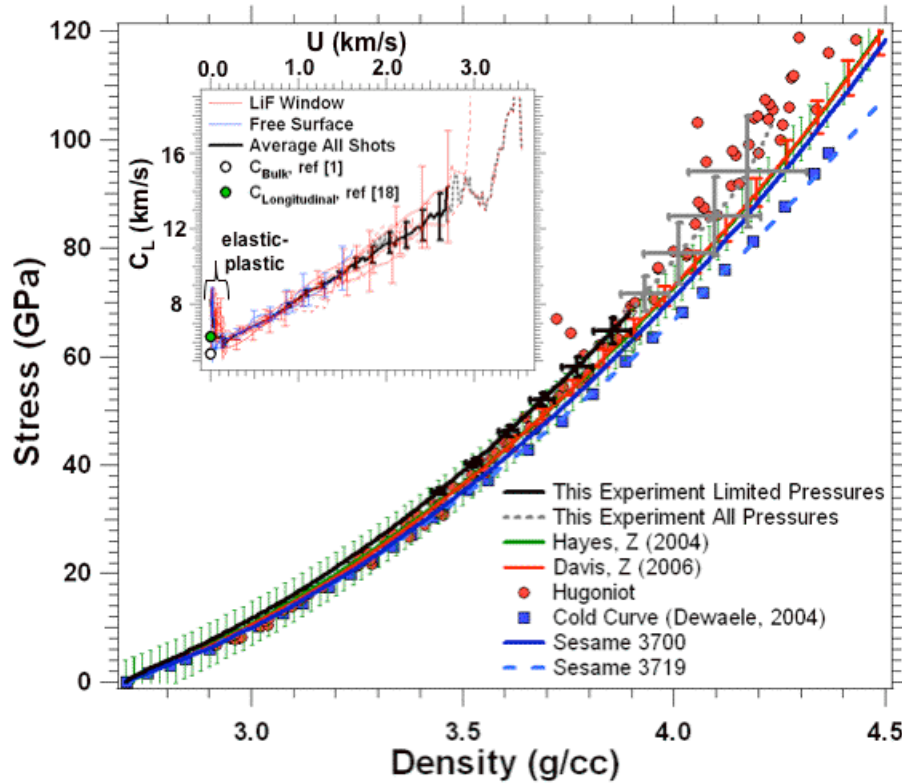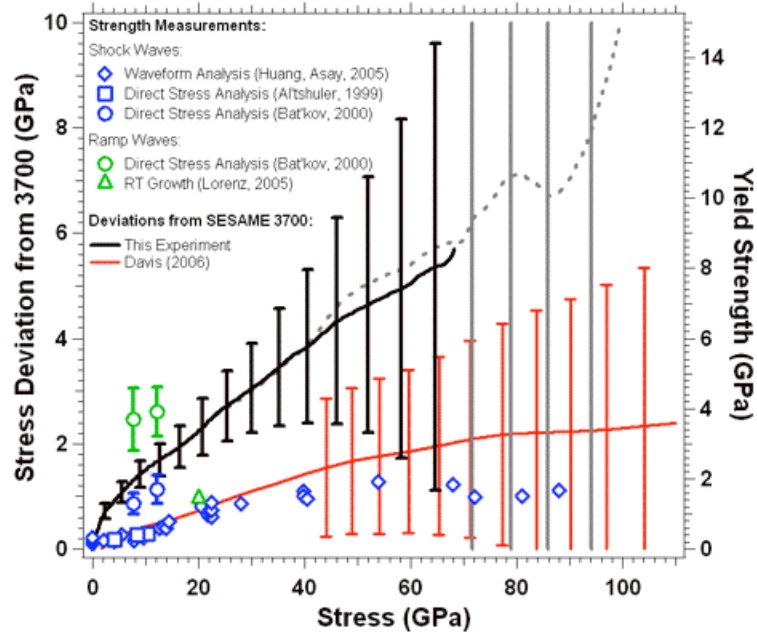
Smith, Figure 1a
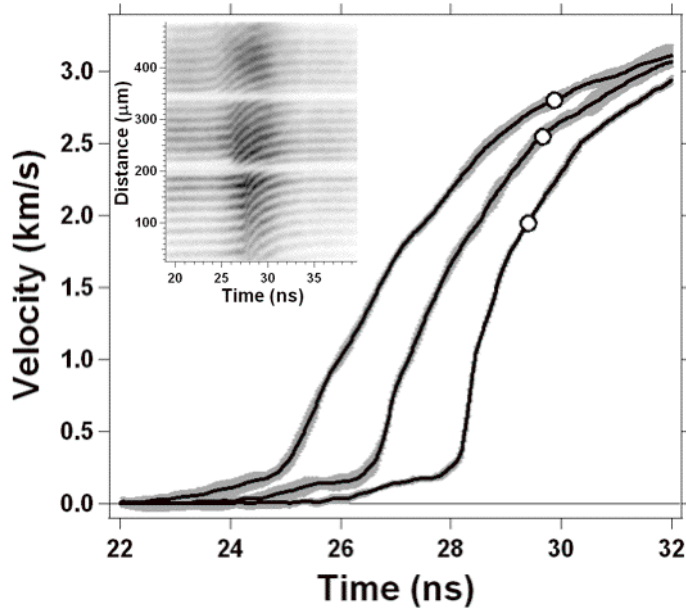
Smith, Figure 1b

Fig 1. (a) X-ray-driven laser ICE-EOS target sketch. (b) Interface velocity history for each step of the Al/LiF example. The width of the curves shows the random uncertainty of the measurement. The black line shows the forward propagated velocity determined from the load pressure history and the measured $C_L(u)$.

Fig 2. Quasi-isentropic stress vs density data presented here together with previous data from Hayes [8] and Davis [11]. Also shown are Hugoniot [2] and cold curve data [19], and calculated isentropes from two different EOS models from the Sesame database [20]. Insert shows $C_L(u)$ for all seven shots. The black line represents the weighted mean $\overline{C_L(u)}$ for all shots with the analysis limited to times preceding the influence of the LiF shock or reverberations in the case of Al/vacuum targets. The grey dashed line represents the weighted mean over the entire profile.

Fig 3. Extra stress versus nominal stress determined by subtracting our measured quasi-isentrope from the isentrope calculated from the table 3700 from the Sesame library. The right hand axis is the same but magnified by 3/2 to enable comparison with previous flow strength results. Also shown are the strength measurements from shock waves of Huang [22], Altshular [23], and Batkov [24], and ramp load data from Lorenz [10] and Batkov [24]. The black (grey) line corresponds to the analysis region described for $C_L(u)$ insert plot in Fig. 2.